Coupling Strategies for Finite Element Modeling of Thermal Elastohydrodynamic Lubrication Problems

W. Habchi*

Lebanese American University, Department of Industrial and Mechanical Engineering, Byblos, Lebanon

*Corresponding author: wassim.habchi@lau.edu.lb

Abstract

This paper investigates coupling strategies for finite element modeling of thermal elastohydrodynamic lubrication (TEHL) problems. The TEHL problem involves a strong coupling between several physics: solid mechanics, fluid mechanics and heat transfer. Customarily, this problem is split into two parts (elastohydrodynamic (EHD) and thermal) and the two problems are solved separately while an iterative procedure is established between their respective solutions. This weak coupling strategy involves a loss of information, as each problem is not made intimately aware of the evolution of the other problem's solution during the resolution procedure. This typically leads to slow convergence rates. The current work offers a full coupling strategy for the TEHL problem i.e. both the EHD and thermal parts are solved simultaneously in a monolithic system. The system of equations is generated from a finite element discretization of the governing field variables: hydrodynamic pressure, solids elastic deformation and temperature. The full coupling strategy prevents any loss of information during the resolution procedure leading to very fast convergence rates (solution is attained within a few iterations only). The performance of the full coupling strategy is compared to that of different weak coupling strategies. Out of simplicity, only steady-state line contacts are considered in this work. Nevertheless, the proposed methodology, results and findings are of a general nature and may be extrapolated to circular or elliptical contacts under steady-state or transient conditions.

Keywords: Thermal Elastohydrodynamic Lubrication; Numerical Modeling; Coupling Strategies; Finite Elements;

1. Introduction

Elastohydrodynamic lubrication (EHL) has grown to become a fully-fledged scientific field owing to its importance for a proper and safe operation of many moving machine elements such as gears, bearings, cam-followers, etc. Elastohydrodynamic (EHD) contacts are lubricated contacts in which the contacting solids are fully separated by a lubricant film inside which the generated hydrodynamic pressures are high enough to induce an elastic deformation of the solid

components. Pressures may be as high as several GPa, film thicknesses as low as a few nm and shear stresses within the lubricant film may reach hundreds of MPa. Under such conditions, the Newtonian limit of most lubricants is exceeded and significant heat generation by shear may occur within EHL conjunctions leading to a temperature rise that may exceed 100^{o}C in extreme cases. As such, it becomes inevitable for any numerical model for simulating EHL contacts to account for the non-Newtonian response of the lubricant as well as the dissipation of heat within the lubricant film and contacting solids. This is essential for an accurate prediction of lubricant film thickness and friction generation within these contacts.

Over the years, many numerical models of thermal non-Newtonian EHL lubrication have emerged. One of the pioneering works on the topic is that of Cheng and his co-workers [1] [2] who were the first to incorporate thermal effects into the numerical solution of the EHL line contact problem. The first full numerical solution of the point contact problem under TEHL conditions was obtained by Zhu and Wen [3]. Many other researchers developed different numerical tools for the simulation of the TEHL problem such as Kim and Sadeghi [4], Guo et al. [5], Liu et al. [6] or also Sharif et al. [7] who solved the full energy equation in order to obtain the temperature distribution throughout the lubricant film. The contacting solids though, were not included in the thermal analysis. Instead, temperature at the solid-fluid interfaces is imposed as an essential boundary condition and is obtained based on the full expression for a moving heat source given by Carslaw and Jaeger [8]. The latter is obtained from a direct analogy with Blok's [9] flash temperature concept derived for solid-to-solid contacts. Another type of TEHL models that employed this simplification is that of Hartinger et al. [10] who solved the problem using a Computational Fluid Dynamics (CFD) approach. The latter consists in solving the full Navier-Stokes equations for the hydrodynamic part instead of the simplified Reynolds equation using a finite volume discretization. However, the heavy computational overhead associated with CFD models remains prohibitive and most often limits this kind of approach to the line contact configuration. A further simplification has been adopted in many works consisting in assuming a parabolic temperature profile across the lubricant film thickness. This reduces the dimension of the thermal problem by one and avoids the heavy computational cost associated with the discretization across the film required by the energy equation. Examples of such works are that of Salehizadeh and Saka [11], Wolff and Kubo [12], and Kazama et al. [13] for the line contact problem or also Jiang et al. [14], Lee et al. [15] and Kim et al. [16] [17] for the point contact problem. However, the parabolic temperature profile simplification leads to inaccurate predictions in the contact inlet as shown in [13]. This is due to the occurrence of complex thermal convective effects that are associated with significant reverse flows appearing in this region of the contact. Other works such as that of Kaneta et al. [18] or also Wang et al. [19] incorporated the solid components into their thermal analysis which is based on the solution of the full energy equation applied to the solids and lubricant film. Most of the above mentioned TEHL models are based on a finite difference discretization of the governing partial differential equations (Reynolds and energy equation). More recently, Habchi et al. [20] [21] introduced a finite element model (FEM) for thermal elastohydrodynamic lubrication incorporating the solid

components into both the EHL and thermal parts of the model. This allowed a later incorporation of complex effects such as surface coatings [22] [23] into the model. They also solved the full energy equation in both the solid and lubricant domains. In addition, the use of finite elements allowed the adoption of non-regular non-structured meshing of the geometric domains of the solids and lubricant film leading to significant reductions in computational overheads.

A common aspect of all the above cited TEHL models is the partition of the problem into two parts: EHL and thermal. These two problems are solved separately and an iterative procedure is established between their respective solutions until convergence is attained. This weak coupling strategy involves a loss of information, as each problem is not made intimately aware of the evolution of the other problem's solution during the resolution procedure. This typically leads to slow convergence rates. Up to the author's knowledge, the only work to have offered a full coupling of the TEHL problem is that of Bruyere et al. [24]. However, it is based on a CFD approach which, as stated earlier, is associated with heavy computational costs and this is probably why only line contacts were considered. Such models are based on the solution of the full Navier-Stokes equations for the hydrodynamic part of the problem instead of the simplified Reynolds equation. This allows, under certain operating conditions, a better capture of the complex reverse flows occurring in the inlet region of the contact as highlighted by Hartinger et al. [10]. However, under most conditions, the simplified Reynolds equation, which is directly derived from the Navier-Stokes equations by applying thin film approximations, succeeds in predicting these reverse flows with reasonable accuracy. This being said, the extra computational cost associated with CFD approaches remains prohibitive and does not justify their use as a replacement to the much less computationally demanding Reynolds-based ones especially that both allow perfectly comparable pressure, film thickness and friction predictions.

The merits of full coupling have been praised by Habchi et al. [21] [25] for the isothermal Newtonian EHD problem. In fact, the latter is based on the solution of the Reynolds, linear elasticity and load balance equations. Most isothermal Newtonian EHD models in the literature solve these equations separately (weak coupling) and an iterative procedure is established between their respective solutions. The very few models that adopted a full coupling strategy [26] [27] [28] [29] suffered from two major limitations. First, the simultaneous solution of all pressure updates meant a tedious implementation of the cavitation boundary condition at the exit of the contact and second, the use of the half-space approach to compute the elastic deformation of the contacting solids lead to a full Jacobian matrix arising in the solution of the corresponding algebraic non-linear system of equations. The computational overhead associated with the inversion of this full Jacobian matrix turned out to be prohibitive. An alternative, the "differential deflection method", was offered by Evans and Hughes [30] and consisted in deriving a differential equation from the half-space approach with a more localized character and a less dense Jacobian matrix. However, it remained relatively dense for the point contact case [31] and the arising Jacobian matrix had a relatively large bandwidth. This required a special iterative technique to be used in order to solve the fully coupled equations efficiently. Habchi et al. [21]

[25] offered solutions to the limitations associated with fully coupled isothermal Newtonian EHD models. The problem of the tedious implementation of the cavitation boundary condition was overcome by adopting a penalty method as proposed by Wu [32] while the problem of the full Jacobian matrix was solved by using a classical linear elasticity approach to compute the elastic deformation of the contacting solids leading to a sparse Jacobian matrix. This allowed the authors to establish an efficient full coupling strategy for the isothermal Newtonian EHD problem. It was shown that a full coupling strategy enables much faster convergence rates allowing the solution to be attained within a few iterations instead of hundreds. The authors extended their proposed model to include thermal and non-Newtonian effects [20] [21]. However, the EHL part was solved in a fully coupled way while full coupling between the EHL and thermal parts was yet to be established. The current work attempts to fill this gap by providing a fully coupled finite element TEHD model using a Reynolds-based approach for the hydrodynamic part of the problem. The fast convergence features associated with full coupling are revealed. A thorough comparison between full coupling and different weak coupling strategies, in terms of computational cost and memory requirements, is also carried out.

2. Governing Equations

This part describes the governing equations of the TEHL problem. For the sake of simplicity, only steady-state line contacts are considered in this work. However, the proposed methodology and results are of a general nature and can be extended to the more general case of circular or elliptical contacts under steady-state or transient conditions. The geometry of a line contact can be reduced to that of a contact between a cylinder of radius R and infinite length with a flat plane (half-space) as shown in figure 1. From this point on, the subscripts c and p are used to represent the cylinder and plane respectively and the subscript f is used for the fluid (lubricant).

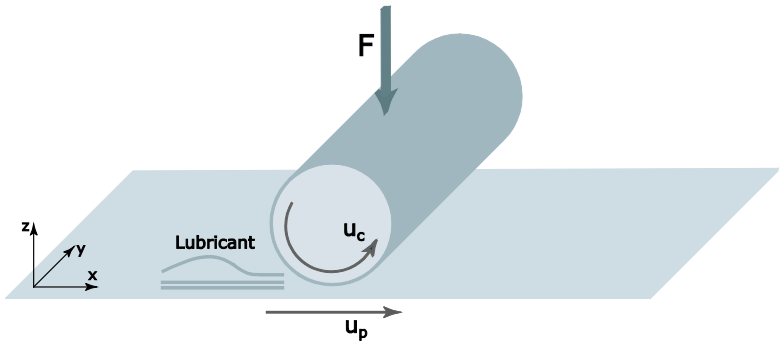

Figure 1: Geometry of a line contact

The solid surfaces are assumed to be smooth and to be moving at constant unidirectional surface velocities u_c and u_p in the x-direction. A full lubricant film is assumed to separate the two solids that are pressed against each other by a constant external applied force F. The lubricant is assumed to have a generalized-Newtonian behavior. The model description is split into two parts: the EHL part describing the lubricant flow and elastic deformation of the solids

and the thermal part describing the heat dissipation within the EHL conjunction. All equations provided in this section are written in dimensionless form using Hertzian contact parameters.

2.1 EHL Part

The EHL part describes the flow of lubricant through the deformed EHL conjunction. Since the length of the contact is infinite in the *y*-direction, the variations of all governing field variables in this direction are nil. Hence, the geometrical domain Ω for this part is two-dimensional in the *xz*-plane. It is represented by a square of sufficient size to ensure a half-space configuration as shown in figure 2. Habchi et al. [25] showed that a dimensionless side length of 60 is sufficient to ensure zero displacement in the regions far away from the 1D contact zone $\partial\Omega_c$. The latter is located on the upper side of the square and has a dimensionless length of 6.

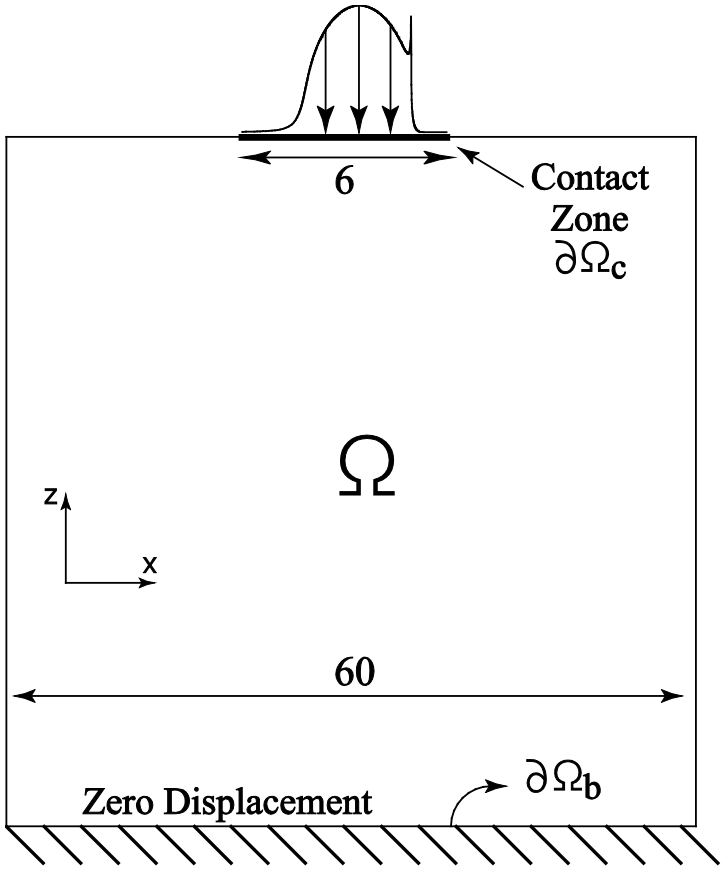

Figure 2: Computational domain of the EHL Part

The dimensionless hydrodynamic pressure *P* generated within the EHL conjunction is governed by the generalized Reynolds equation proposed by Yang and Wen [33]:

$$-\frac{\partial}{\partial X}\left(\bar{\varepsilon}\,\frac{\partial P}{\partial X}\right)+\frac{\partial\left(\bar{\rho}^{*}H\right)}{\partial X}=0$$

Where:

$$\bar{\varepsilon}=\left(\frac{\bar{\rho}}{\bar{\eta}}\right)_e\frac{H^3}{\lambda};\qquad \left(\frac{\bar{\rho}}{\bar{\eta}}\right)_e=\frac{\bar{\eta}_e\bar{\rho}'_e}{\bar{\eta}'_e}-\bar{\rho}''_e \quad\text{and}\quad \lambda=\frac{u_m R^2\mu_{1,R}}{a^3 p_h} \quad\text{with}\quad u_m=\frac{u_p+u_c}{2}$$

$$\bar{\rho}^{*}=\frac{\left[\bar{\rho}'_e\bar{\eta}_e\left(u_c-u_p\right)+\bar{\rho}_e u_p\right]}{u_m};\qquad \bar{\rho}_e=\int_0^1\bar{\rho}\,dZ$$

$$\bar{\rho}'_e=\int_0^1\bar{\rho}\int_0^Z\frac{dZ'}{\bar{\eta}}dZ;\qquad \bar{\rho}''_e=\int_0^1\bar{\rho}\int_0^Z\frac{Z'dZ'}{\bar{\eta}}dZ$$

$$\frac{1}{\bar{\eta}_e}=\int_0^1\frac{dZ}{\bar{\eta}};\qquad \frac{1}{\bar{\eta}'_e}=\int_0^1\frac{Z\,dZ}{\bar{\eta}} \tag{1}$$

Where Z=0 corresponds to the plane's surface while Z=1 corresponds to the cylinder's surface. This equation is applied to the *1D* contact domain $\partial\Omega_c$ located between X=-4.5 (inlet) and X=1.5 (outlet) on the upper side of the geometrical domain Ω. A zero pressure boundary condition is applied at the inlet and outlet of the contact and the Reynolds' cavitation boundary condition requires that:

$$p\geq 0 \quad\text{on}\quad \Omega_c \quad\text{and}\quad p=\frac{\partial P}{\partial X}=0 \quad\text{on the cavitation boundary} \tag{2}$$

The cavitation boundary condition is handled by using the penalty method proposed by Wu [32]. The latter consists in adding a penalty term to the generalized Reynolds equation which becomes:

$$-\frac{\partial}{\partial X}\left(\bar{\varepsilon}\,\frac{\partial P}{\partial X}\right)+\frac{\partial\left(\bar{\rho}^{*}H\right)}{\partial X}+\underbrace{\xi\;P^{-}}_{\text{Penalty Term}}=0 \tag{3}$$

Where P^{-} corresponds to the negative part of the pressure distribution which can be defined as $P^{-}=P\,\theta(-P)$ (where θ is the Heaviside function which is nil for a negative argument and equal to unity for a positive one). Note that the penalty term has no effect in positive pressure regions and the consistency of the generalized Reynolds equation is preserved. However, in the outlet region of the contact where negative pressures arise, the penalty term dominates equation (3) and forces the negative pressures towards zero provided that the arbitrary constant ξ has a sufficiently large value. The dependence of the dimensionless generalized-Newtonian viscosity $\bar{\eta}$ on dimensionless shear stress $\bar{\tau}=\tau/\tau_0$ could be described by any of the known non-Newtonian models. In this work, the double-Newtonian modified Carreau model [34] is used:

$$\bar{\eta}\left(P,\bar{T},\bar{\tau}\right)=\bar{\mu}_2\left(P,\bar{T}\right)+\frac{\bar{\mu}_1\left(P,\bar{T}\right)-\bar{\mu}_2\left(P,\bar{T}\right)}{\left[1+\left(\frac{\bar{\tau}\,\tau_0}{G_c}\right)^{a_c}\right]^{\frac{\frac{1}{n_c}-1}{a_c}}} \tag{4}$$

Where a_c, n_c and G_c are constants and the choice of $\tau_0 = p_h$ is adopted. The shear stress $\bar{\tau}$ is determined from the solution of the following non-linear equation applied at every point of the contact zone $\partial\Omega_c$:

$$\frac{H\,a^2\,\tau_0}{\mu_{1,R}\,R}\int_0^1\frac{\bar{\tau}}{\bar{\eta}\left(P,\bar{T},\bar{\tau}\right)}dZ=u_c-u_p \qquad \text{with:} \qquad \bar{\tau}=\bar{\tau}_p+\frac{H\,a\,p_h}{R\,\tau_0}Z\frac{\partial P}{\partial X} \tag{5}$$

Where $\bar{\tau}_p$ corresponds to the dimensionless lubricant shear stress on the plane's surface (Z=0). The pressure-temperature dependence of the dimensionless Newtonian viscosities $\bar{\mu}_1$ and $\bar{\mu}_2$ in equation (4) is described by the Roelands [35] equation for simplicity:

$$\bar{\mu}_i\left(P,\bar{T}\right)=\frac{\mu_{i,R}}{\mu_{1,R}}\exp\left\{\left(\ln\left(\mu_R\right)+9.67\right)\left[-1+\left(1+5.1\times10^{-9}\,P\,p_h\right)^{Z_0}\left(\frac{\bar{T}\,T_R-138}{T_R-138}\right)^{-S_0}\right]\right\}$$
$$\text{With:}\quad i=1 \text{ or } 2,\quad Z_0=\frac{\alpha}{\left[5.1\times10^{-9}\left(\ln\left(\mu_R\right)+9.67\right)\right]}\quad\text{and}\quad S_0=\frac{\beta\left(T_R-138\right)}{\ln\left(\mu_R\right)+9.67} \tag{6}$$

Where α is the lubricant's pressure-viscosity coefficient, β its temperature-viscosity coefficient and $\mu_{1,R}$ and $\mu_{2,R}$ its first and second Newtonian viscosity limits at the reference state under zero and infinite shear rates respectively. The reference state throughout this work is chosen to be $P_R = 0$ and $T_R = T_0 = 300K$ ($\bar{T}_R = 1$), where T_0 is the ambient temperature. The dependence of the lubricant's dimensionless density on pressure and temperature is described by the Dowson & Higginson [36] relationship for simplicity:

$$\bar{\rho}\left(P,\bar{T}\right)=\frac{0.59\times10^9+1.34\,P\,p_h}{0.59\times10^9+P\,p_h}-\gamma\,T_R\left(\bar{T}-1\right) \tag{7}$$

Where γ is the lubricant's temperature-density coefficient. The dimensionless film thickness H appearing in equation (1) is expressed as a function of the rigid body separation term H_0 and W (the Z-component of the total dimensionless elastic deformation of the solids in the contact zone $\partial\Omega_c$) as follows:

$$H = H_0 + \frac{X^2}{2} - W(X) \tag{8}$$

Where the middle term on the right-hand-side corresponds to the non-deformed shape of the EHL conjunction. The total elastic deflection of the two solids is obtained by assuming that one of them is rigid while the other is elastic and it accommodates the total deflection of both. Habchi et al. [21] showed that the equivalent modulus of elasticity E and Poisson coefficient υ of the latter are expressed as a function of those of the cylinder and plane as follows:

$$E = \frac{E_p^2 E_c \left(1+\upsilon_c\right)^2 + E_c^2 E_p \left(1+\upsilon_p\right)^2}{\left[E_p\left(1+\upsilon_c\right) + E_c\left(1+\upsilon_p\right)\right]^2} \quad \text{and} \quad \upsilon = \frac{E_p \upsilon_c \left(1+\upsilon_c\right) + E_c \upsilon_p \left(1+\upsilon_p\right)}{E_p\left(1+\upsilon_c\right) + E_c\left(1+\upsilon_p\right)} \tag{9}$$

A classical linear elasticity approach is applied to the solid domain Ω to get the total elastic deflection of the equivalent solid under the applied hydrodynamic pressure P in the contact zone. A plane strain approximation is adopted since the solids have an infinite length in the Y-direction. The governing partial differential equations can be written as a function of the total dimensionless elastic deflection components U and W of the elastic deformation field $\bar{U}$ in the X and Z-directions respectively:

$$\begin{cases} -\dfrac{\partial}{\partial X}\left[C_1 \dfrac{\partial U}{\partial X} + C_2 \dfrac{\partial W}{\partial Z}\right] - \dfrac{\partial}{\partial Z}\left[C_3\left(\dfrac{\partial U}{\partial Z} + \dfrac{\partial W}{\partial X}\right)\right] = 0 \\ -\dfrac{\partial}{\partial X}\left[C_3\left(\dfrac{\partial U}{\partial Z} + \dfrac{\partial W}{\partial X}\right)\right] - \dfrac{\partial}{\partial Z}\left[C_2 \dfrac{\partial U}{\partial X} + C_1 \dfrac{\partial W}{\partial Z}\right] = 0 \end{cases}$$

With: (10)

$$C_1 = \frac{E(1-\upsilon)}{(1+\upsilon)(1-2\upsilon)} \frac{a}{R\, p_h}, \quad C_2 = \frac{\upsilon E}{(1+\upsilon)(1-2\upsilon)} \frac{a}{R\, p_h} \quad \text{and} \quad C_3 = \frac{E}{2(1+\upsilon)} \frac{a}{R\, p_h}$$

This equation can be re-arranged in a more compact form as a function of the dimensionless stress tensor σ and dimensionless strain tensor ε:

$$-\nabla \cdot \sigma = 0$$

Where: $\sigma = \begin{bmatrix} \sigma_{XX} & \sigma_{XZ} \\ \sigma_{XZ} & \sigma_{ZZ} \end{bmatrix}$ can be re-arranged using Voigt's notation as:

$$\begin{Bmatrix} \sigma_{XX} \\ \sigma_{ZZ} \\ \sigma_{XZ} \end{Bmatrix} = \underbrace{\begin{bmatrix} C_1 & C_2 & 0 \\ C_2 & C_1 & 0 \\ 0 & 0 & C_3 \end{bmatrix}}_{C} \begin{Bmatrix} \varepsilon_{XX} \\ \varepsilon_{ZZ} \\ \varepsilon_{XZ} \end{Bmatrix} \quad \text{or} \quad \sigma = C\varepsilon\left(\bar{U}\right) \tag{11}$$

with: $\varepsilon\left(\bar{U}\right) = D\bar{U}$ where $D = \begin{bmatrix} \frac{\partial}{\partial X} & 0 \\ 0 & \frac{\partial}{\partial Z} \\ \frac{\partial}{\partial Z} & \frac{\partial}{\partial X} \end{bmatrix}$ and $\bar{U} = \begin{Bmatrix} U \\ W \end{Bmatrix}$

A zero displacement boundary condition is applied to $\partial\Omega_b$ while the dimensionless hydrodynamic pressure *P* is applied as a dimensionless normal stress $\bar{\sigma}_n$ over the contact domain $\partial\Omega_c$:

$$\bar{\sigma}_n = \sigma_{ZZ} = C_2 \frac{\partial U}{\partial X} + C_1 \frac{\partial W}{\partial Z} = -P \tag{12}$$

A free displacement boundary condition ($\bar{\sigma}_n = \bar{\sigma}_t = 0$) is applied to the remainder of the boundaries of Ω. Finally, to complete the EHL part, the load balance equation in dimensionless form reads:

$$\int_{\partial\Omega_c} P \, dX = \frac{\pi}{2} \tag{13}$$

This equality ensures equilibrium of forces between the external applied load and the hydrodynamic pressure generated within the lubricant film. This is done by monitoring the value of the rigid body separation term H_0 as explained later.

2.2 Thermal Part

The thermal part describes the heat generation and dissipation through the lubricant film and bounding solids. Since the length of the contact is infinite in the *Y*-direction, temperature variations are nil in this direction. Hence, the geometrical domain for this part is two-dimensional in the *XZ*-plane. It is represented by three adjacent rectangular domains as shown in figure 3: Ω_f for the fluid domain sandwiched between Ω_p for the plane and Ω_c for the cylinder.

For the solid domains, Kaneta et al. [18] and Wang et al. [19] showed that a dimensionless depth of 3.15 is enough in most cases to ensure a zero temperature gradient in regions that are far from the fluid-solid interfaces. In this work, a dimensionless depth of 3.5 is adopted. As for the fluid domain, it has a unit height since $Z = z/h$.

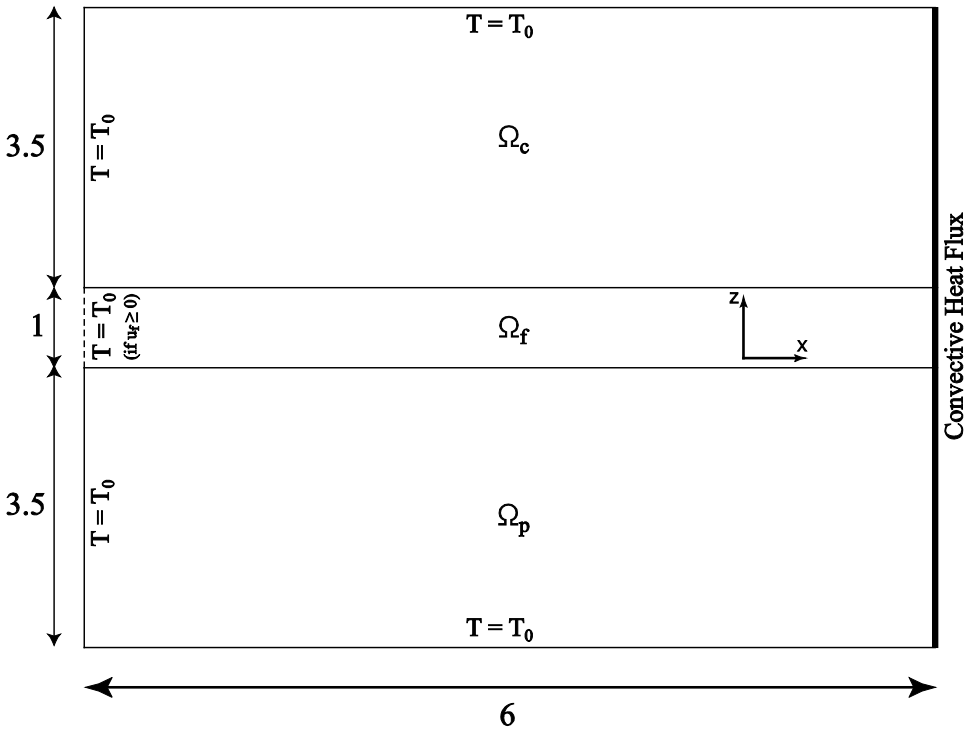

Figure 3: Computational domain of the thermal Part

The heat flow within the lubricant film and solids is governed by the energy equation applied to their respective domains. In dimensionless form, after a few manipulations, the corresponding equations read:

$$\begin{cases} -\dfrac{\partial}{\partial X}\left(\dfrac{k_p}{a}\dfrac{\partial \overline{T}}{\partial X}\right)-\dfrac{\partial}{\partial Z}\left(\dfrac{k_p}{a}\dfrac{\partial \overline{T}}{\partial Z}\right)+\rho_p c_p u_p \dfrac{\partial \overline{T}}{\partial X}=0 & \text{(Solid } p\text{)} \\ -\dfrac{\partial}{\partial X}\left(\dfrac{k_c}{a}\dfrac{\partial \overline{T}}{\partial X}\right)-\dfrac{\partial}{\partial Z}\left(\dfrac{k_c}{a}\dfrac{\partial \overline{T}}{\partial Z}\right)+\rho_c c_c u_c \dfrac{\partial \overline{T}}{\partial X}=0 & \text{(Solid } s\text{)} \\ -\dfrac{\partial}{\partial X}\left(\dfrac{kH}{R}\dfrac{\partial \overline{T}}{\partial X}\right)-\dfrac{\partial}{\partial Z}\left(\dfrac{kR}{Ha^2}\dfrac{\partial \overline{T}}{\partial Z}\right)+\rho_R \overline{\rho}\, c\, u_f \dfrac{Ha}{R}\dfrac{\partial \overline{T}}{\partial X}=Q_{comp}+Q_{shear} & \text{(Lubricant film)} \end{cases} \tag{14}$$

With: $Q_{comp} = -\dfrac{H\, a\, p_h}{RT_0}\dfrac{\overline{T}}{\overline{\rho}}\dfrac{\partial \overline{\rho}}{\partial \overline{T}} u_f \dfrac{\partial P}{\partial X}$ and $Q_{shear} = \dfrac{\overline{\eta}\mu_{1,R} Ha^2}{RT_0}\dot{\gamma}_{zx}^2$

Note that heat convection within the lubricant film in the *Z*-direction is neglected since the lubricant velocity component in that direction is negligible according to the thin film assumptions. The right-hand-side terms for the lubricant film energy equation correspond to heat

generation within the lubricant film by compression (Q_{comp}) and by shear (Q_{shear}). The lubricant velocity component in the *x*-direction u_f is expressed as:

$$u_f = u_p + \frac{p_h H^2 a^3}{R^2 \mu_{1,R}} \frac{\partial P}{\partial X} \left[\int_0^Z \frac{Z' dZ'}{\bar{\eta}} - \frac{\bar{\eta}_e}{\bar{\eta}_e'} \int_0^Z \frac{dZ}{\bar{\eta}} \right] + \bar{\eta}_e \left(u_c - u_p \right) \int_0^Z \frac{dZ}{\bar{\eta}} \tag{15}$$

And the lubricant shear rate through the film thickness $\dot{\gamma}_{zx}$ in the *x*-direction is defined as follows:

$$\dot{\gamma}_{zx} = \frac{\partial u_f}{\partial z} = \frac{Ha p_h}{\mu_{1,R} \bar{\eta} R} \frac{\partial P}{\partial X} \left(Z - \frac{\bar{\eta}_e}{\bar{\eta}_e'} \right) + \frac{R}{Ha^2} \frac{\bar{\eta}_e}{\bar{\eta}} \left(u_c - u_p \right) \tag{16}$$

Equations (14) can be rewritten in a more compact form as follows:

$$-\nabla \cdot \left(\vec{k} \cdot \nabla \bar{T} \right) + \varphi \frac{\partial \bar{T}}{\partial X} = Q \quad \text{with} \quad \vec{k} = \begin{bmatrix} k_x & 0 \\ 0 & k_z \end{bmatrix} \tag{17}$$

For the plane domain $k_x = k_z = k_p / a$, $\varphi = \rho_p c_p u_p$ and $Q = 0$ as for the cylinder domain $k_x = k_z = k_c / a$, $\varphi = \rho_c c_c u_c$ and $Q = 0$. For the fluid domain, $k_x = kH/R$, $k_z = kR/Ha^2$, $\varphi = \rho_R \bar{\rho}\, c\, u_f Ha/R$ and $Q = Q_{comp} + Q_{shear}$. The boundary conditions associated with the thermal problem are shown in figure 3. Heat flux continuity boundary conditions are imposed on the two fluid-solid interfaces as follows:

$$\frac{k_p}{a} \frac{\partial \bar{T}}{\partial Z}\bigg|_{Z=0^-} = \frac{kR}{Ha^2} \frac{\partial \bar{T}}{\partial Z}\bigg|_{Z=0^+} \quad \text{and} \quad \frac{k_c}{a} \frac{\partial \bar{T}}{\partial Z}\bigg|_{Z=1^+} = \frac{kR}{Ha^2} \frac{\partial \bar{T}}{\partial Z}\bigg|_{Z=1^-} \tag{18}$$

An ambient temperature T_0 is imposed ($\bar{T} = 1$) on all inlets (left side of the computational domain) since the energy equation is hyperbolic (owing to the convective terms). Note that for the solids, u_c and u_p are assumed to be positive throughout this work and the left boundaries are actual inlet boundaries. However, for the lubricant film, because of the reverse flows occurring in the inlet region of the contact, u_f may be negative on the left side boundary and therefore the ambient temperature boundary condition only needs to be imposed on inlet sections (where $u_f \geq 0$). An ambient temperature T_0 is also imposed in the depth of the solids (top and bottom boundaries). As for the outlet boundaries (right side) of the solids and lubricant film, a convective heat flux boundary condition is assumed. That is, the conductive heat flux ($\left(\vec{k} \cdot \nabla \bar{T} \right)^T \cdot \vec{n}$, where $\vec{n}$ is a normal outward unit vector) is assumed to be nil.

3. Finite Element Model

The TEHL problem for line contacts is governed by the system of equations formed by the generalized Reynolds equation (3), the linear elasticity equations (11), the load balance equation (13), the energy equations (17) and the shear stress equation (5). Equation (3) governs the hydrodynamic pressure build-up within the EHL conjunction. The associated unknown field variable is the *1D* dimensionless pressure distribution P over the contact zone $\partial\Omega_c$ and the subscript h (for "hydrodynamic") will be associated to it. The system of equations (11) governs the elastic deformation of the solid components under the applied contact pressure. The associated unknown field variable is the *2D* dimensionless total elastic deformation field $\bar{U}$ over the solid domain Ω and the subscript e (for "elastic") will be associated to it. Equation (13) defines the equilibrium of forces over the contact and is written as a function of P. However, the associated unknown field variable is the scalar rigid body separation term H_0. In fact, this equation is added to the system of TEHL equations as an ordinary integral equation while introducing H_0 as an additional unknown. The subscript l (for "load balance") will be associated to it. The system of equations (17) describes the heat flow within the solids and lubricant film. The associated unknown field variable is the *2D* dimensionless temperature distribution $\bar{T}$ over the solid domains Ω_c and Ω_p and the lubricant domain Ω_f. The subscript t (for "thermal") will be associated to this part. And finally, equation (5) defines the shear stress distribution within the lubricant film. This equation is a non-linear integral equation applied at every point of the contact zone $\partial\Omega_c$ to determine the corresponding dimensionless shear stress $\bar{\tau}_p$ at the plane's surface. Therefore, the associated unknown field variable is the *1D* distribution of dimensionless shear stress $\bar{\tau}_p$ at the plane's surface and the subscript s (for "shear stress") will be associated to it. Note that equations (5) and (13) are ordinary integral equations that are directly added to the system of equations along with the introduction of their corresponding field variables as additional unknowns. On the other hand, equations (3), (11) and (17) are partial differential equations requiring a finite element treatment for their solution. A standard Galerkin formulation is applied to these equations. The latter is obtained by multiplying each equation by a corresponding weighting function: N_P for the generalized Reynolds equation, $N_{\bar{U}} = \left\{ N_U \vec{i}, N_W \vec{k} \right\}^T$ for the linear elasticity equations (where $\vec{i}$ and $\vec{k}$ are unit basis vectors in the x and z-directions respectively) and $N_{\bar{T}}$ for the energy equations. Then, each equation is integrated over its domain of application and integration by parts is applied to reveal the natural boundary conditions. For the sake of simplicity, the zero boundary integral terms will be omitted here and the finite element formulation for the TEHL system of equations reads:

Find $\left(P,\bar{U},H_0,\bar{T},\bar{\tau}_p\right)$ such that $\forall\left(N_P,N_{\bar{U}},N_{\bar{T}}\right)$, one has:

$$\begin{cases} \int_\Omega \varepsilon\left(N_{\bar{U}}\right)^T C\ \varepsilon\left(\bar{U}\right)d\Omega+\int_{\partial\Omega_c} P\,N_W\,\vec{n}\,d\Omega=0 \\ \int_{\partial\Omega_c}\left(\bar{\varepsilon}\,\dfrac{\partial P}{\partial X}\dfrac{\partial N_P}{\partial X}-\bar{\rho}^* H\,\dfrac{\partial N_P}{\partial X}+\xi\,P^- N_P\right)d\Omega=0 \\ \int_{\partial\Omega_c} P\,d\Omega-\dfrac{\pi}{2}=0 \\ \int_{\Omega_{p/c/f}}\left(\nabla N_{\bar{T}}{}^T\cdot\vec{k}\cdot\nabla\bar{T}+\varphi\dfrac{\partial\bar{T}}{\partial X}N_{\bar{T}}-Q\,N_{\bar{T}}\right)d\Omega=0 \\ \dfrac{Ha^2}{\mu_{1,R}R}\int_0^1\dfrac{\bar{\tau}_p\tau_0+\dfrac{H\,a\,p_h}{R}Z\dfrac{\partial P}{\partial X}}{\bar{\eta}\left(P,\bar{T},\bar{\tau}\right)}dZ=u_c-u_p \qquad \text{(at every point of } \partial\Omega_c) \end{cases} \tag{19}$$

The penalty term coefficient ξ is defined over a given element Ω_e of $\partial\Omega_c$ as $\xi=10^6\times h_e$, where h_e is the length of Ω_e [21]. Note that for highly loaded contacts, the generalized Reynolds equation gives rise to numerical oscillations in the pressure distribution when a standard Galerkin formulation is employed. Habchi et al. [21] explained that these oscillations appear because the generalized Reynolds equation can be written as a classical convection-diffusion equation in which convection becomes dominant for highly loaded contacts. The inability of the standard Galerkin formulation to resolve fine error scales under convection dominated regime is well known in the FEM literature and special stabilized formulations have been developed over the years to overcome this limitation. In [21], the authors used well-known stabilized FEM formulations such as Streamline Upwind Petrov Galerkin (SUPG) [37] or Galerkin Least Squares (GLS) [38] to remove these oscillations. These require the addition of some residual terms to the standard Galerkin formulation which preserve the consistency of the original equation. Similar stabilizing terms are added to the energy equations of the solids and lubricant film under high speed conditions, in which case heat convection also becomes dominant over conduction. Adding the SUPG stabilizing terms to the generalized Reynolds and energy equations, the system of equations (19) becomes:

Find $\left(P,\bar{U},H_0,\bar{T},\bar{\tau}_p\right)$ such that $\forall\left(N_P,N_{\bar{U}},N_{\bar{T}}\right)$, one has:

$$
\begin{cases}
\displaystyle\int_\Omega \varepsilon\left(N_{\bar{U}}\right)^T\, C\; \varepsilon\left(\bar{U}\right) d\Omega + \int_{\partial\Omega_c} P\, N_W\, \vec{n}\, d\Omega = 0 \\
\displaystyle\int_{\partial\Omega_c}\left(\bar{\varepsilon}\,\frac{\partial P}{\partial X}\frac{\partial N_P}{\partial X} - \bar{\rho}^* H\,\frac{\partial N_P}{\partial X} + \xi\, P^- N_P\right) d\Omega \\
\qquad\qquad + \underbrace{\displaystyle\sum_{e=1}^{n_h}\int_{\partial\Omega_{c,e}} \tau_h\left(H\,\frac{\partial\bar{\rho}^*}{\partial P}\frac{\partial N_P}{\partial X}\right) R_h\, d\Omega}_{SUPG\ term} = 0 \\
\displaystyle\int_{\partial\Omega_c} P\, d\Omega - \frac{\pi}{2} = 0 \\
\displaystyle\int_{\Omega_{p/c/f}}\left(\nabla N_{\bar{T}}{}^T\cdot\vec{k}\cdot\nabla\bar{T} + \varphi\frac{\partial\bar{T}}{\partial X}N_{\bar{T}} - Q\,N_{\bar{T}}\right) d\Omega \\
\qquad\qquad + \underbrace{\displaystyle\sum_{e=1}^{n_t}\int_{\Omega_{p/c/f,e}} \tau_t\left(\varphi\frac{\partial N_{\bar{T}}}{\partial X}\right) R_t\, d\Omega}_{SUPG\ term} = 0 \\
\dfrac{Ha^2}{\mu_{1,R}R}\displaystyle\int_0^1 \frac{\bar{\tau}_p\tau_0 + \dfrac{H\,a\,p_h}{R}Z\dfrac{\partial P}{\partial X}}{\bar{\eta}\left(P,\bar{T},\bar{\tau}\right)} dZ = u_c - u_p \qquad \text{(at every point of } \partial\Omega_c\text{)}
\end{cases}
\tag{20}
$$

Note that the stabilizing terms are added to the interiors $\partial\Omega_{c,e}$, $\Omega_{p,e}$, $\Omega_{c,e}$ and $\Omega_{f,e}$ of all elements *e* of the hydrodynamic and thermal problems which total numbers are denoted n_h and n_t respectively. The terms R_h and R_t correspond to the residuals of the hydrodynamic and thermal problems respectively. The tuning parameters τ_h and τ_t are defined according to the formulation provided by Galeão et al. [39]:

$$
\tau_h = \frac{h_e\left(\coth\left(Pe_h\right) - \dfrac{1}{Pe_h}\right)}{2\left|H\,\dfrac{\partial\bar{\rho}^*}{\partial P}\right| l_h} \quad\text{and}\quad \tau_t = \frac{h_e\left(\coth\left(Pe_t\right) - \dfrac{1}{Pe_t}\right)}{2|\varphi|\,l_t}
$$

$$
\text{with: } Pe_h = \frac{\left|H\,\dfrac{\partial\bar{\rho}^*}{\partial P}\right| h_e}{2\,\bar{\varepsilon}\,l_h} \quad\text{and}\quad Pe_t = \frac{|\varphi|\,h_e}{2\,k_x\,l_t}
\tag{21}
$$

Where h_e corresponds to the characteristic length of a given element *e*, Pe_h and Pe_t are the Peclet numbers which define the convection-to-diffusion ratios for the hydrodynamic and thermal problems respectively while l_h and l_t correspond to the orders of interpolation functions associated to elements of the hydrodynamic and thermal problems respectively. Typically, a

standard Galerkin formulation gives rise to numerical oscillations in the solution of convection-diffusion problems whenever the value of Peclet number exceeds unity, that is, whenever convection dominates conduction. The system of equations (20) is non-linear and thus its resolution requires a special treatment. It is solved using a Newton-like procedure. The latter gives rise to a linearized system of equations in which the unknowns are the increments of the field variables $\delta\bar{U}$, δP, δH_0, $\delta\bar{T}$ and $\delta\bar{\tau}_p$. These are discretized in the usual finite element sense and the arising overall linearized matrix system to be solved at every Newton iteration *i* as a function of the nodal values of the unknown increments of the field variables is of the form:

$$\left[\begin{array}{c|c|c|c|c} K_{ee} & K_{eh} & \varnothing & \varnothing & \varnothing \\ \hline K_{he} & K_{hh} & K_{hl} & K_{ht} & K_{hs} \\ \hline \varnothing & K_{lh} & \varnothing & \varnothing & \varnothing \\ \hline K_{te} & K_{th} & K_{tl} & K_{tt} & K_{ts} \\ \hline K_{se} & K_{sh} & K_{sl} & K_{st} & K_{ss} \end{array}\right]^{i-1} \left\{\begin{array}{c} \delta\bar{U} \\ \hline \delta P \\ \hline \delta H_0 \\ \hline \delta\bar{T} \\ \hline \delta\bar{\tau}_p \end{array}\right\}^{i} = \left\{\begin{array}{c} \varnothing \\ \hline R_h \\ \hline R_l \\ \hline R_t \\ \hline R_s \end{array}\right\}^{i-1} \tag{22}$$

The matrix on the left-hand-side is the Jacobian matrix to be evaluated at every Newton iteration *i* as a function of the field variables obtained at the previous iteration *i*-1. The right-hand-side is formed by the residual vectors of the hydrodynamic (R_h), load balance (R_l), thermal (R_t) and shear stress (R_s) problems. These are also evaluated at every Newton iteration *i* as a function of the field variables obtained at the previous iteration *i*-1. Note that the residual vector for the elastic problem (R_e) is nill since the linear elasticity equations are linear and the corresponding initial guess is chosen to satisfy them. The starting point for the overall numerical procedure is the selection of appropriate guesses for all the field variables. For *P*, a dimensionless Hertzian pressure distribution is adopted and its corresponding elastic deformation is used to initialize $\bar{U}$. A homogeneous ambient temperature distribution ($\bar{T}=1$) is used to initialize the temperature field and for $\bar{\tau}_p$ an initial guess of zero could be used or a fraction of the Hertzian pressure distribution (typically 5%). Starting from the initial guess, the system of equations (22) is solved for the increments of the field variables using a sparse direct linear system solver (UMFPACK [40]). The equations being highly non-linear, a damped-Newton [41] procedure is employed to ensure convergence. The latter consists in adding at every Newton iteration *i*, a carefully selected fraction $\lambda^i \in]0,1]$ of the solution increments (instead of the full increments) to the solution obtained at the previous iteration *i*-1. The fraction λ^i is computed in such a way to minimize the error at every resolution step and ensure that the obtained solution remains within the relatively narrow convergence radius of Newton's method. This resolution

procedure is repeated until a converged solution is attained. More details about the damped Newton method and its stopping criteria can be found in [41].

4. Results

This section presents typical TEHL results obtained using the full coupling strategy introduced above. The computational performance of the corresponding finite element model is also examined and compared to that of different weak coupling strategies. Throughout this section, steel-on-steel contacts are considered. The properties of the considered steel as well as the lubricant's properties and the operating conditions are summarized in table 1:

Lubricant Properties		Solid Material Properties	Operating Conditions
$\mu_{1,R} = 0.1$ Pa·s	$c = 1500$ J/kg·K	$E_p = E_c = 210$ GPa	$T_R = T_0 = 300$ K
$\mu_{2,R}/\mu_{1,R} = 0.5$ or 0.01	$k = 0.1$ W/m·K	$\upsilon_p = \upsilon_c = 0.3$	$R = 15$ mm
$\alpha = 15$ or 25GPa^{-1}	$G_c = 0.01$ MPa	$\rho_p = \rho_c = 7850$ kg/m^3	$u_m = 0.1$ or 1.0 m/s
$\beta = 0.05$ K^{-1}	$a_c = 2.2$	$k_p = k_c = 46$ W/m·K	$SRR = 0.0$; 0.5 or 1.0
$\gamma = 0.00075$ K^{-1}	$n_c = 0.8$	$c_p = c_c = 470$ J/kg·K	$F = 0.2$ or 2 MN/m
$\rho_R = 750$ kg/m^3			$p_h = 0.7$ or 2.2 GPa

Table 1: Lubricant properties, solid material properties and operating conditions

Note that two loading conditions are considered: a moderate load with $F = 0.2$ MN/m corresponding to a Hertzian contact pressure $p_h = 0.7$ GPa and a high load with $F = 2$ MN/m corresponding to $p_h = 2.2$ GPa. All numerical tests are run on a personal laptop using a single Intel Core i7 - 2.7 GHz processor

4.1. Mesh Selection and Specifications

Five different mesh cases are considered in this work. These are named "*Extra Coarse*", "*Coarse*", "*Normal*", "*Fine*" and "*Extra Fine*" from the coarsest to the finest. All mesh cases are specifically tailored towards the EHL problem. That is, a fine mesh is used in the contact region and its surrounding and the mesh size is progressively increased with distance from the contact region. This is because all field variables exhibit significant variations in the vicinity of the contact region and these variations become smaller and smaller with distance from the latter. Figure 4 shows the "*Extra Coarse*" mesh case for the EHL and thermal domains. Note that non-structured triangular meshing is used for all domains except for the fluid domain in the thermal part where a structured rectangular meshing is employed. This is to allow an easier handling/computation of the density and viscosity integral terms arising in equation (1). A six-point Gauss quadrature rule was found to be sufficiently accurate for the evaluation of these integrals. It is noteworthy to mention that the distancing between points in the *x*-direction for the fluid domain in the thermal part is chosen to exactly map the mesh over the contact region $\partial\Omega_c$ in the EHL part. This is to avoid any unnecessary interpolation operations for the field variables of each part over a non-mapped mesh in the other. Also note that the mesh of the thermal part is

symmetric with respect to an axis passing through the mid-layer of the lubricant film in the *x*-direction. Second order Lagrange interpolation functions are used for all elements in both the EHL and thermal domains.

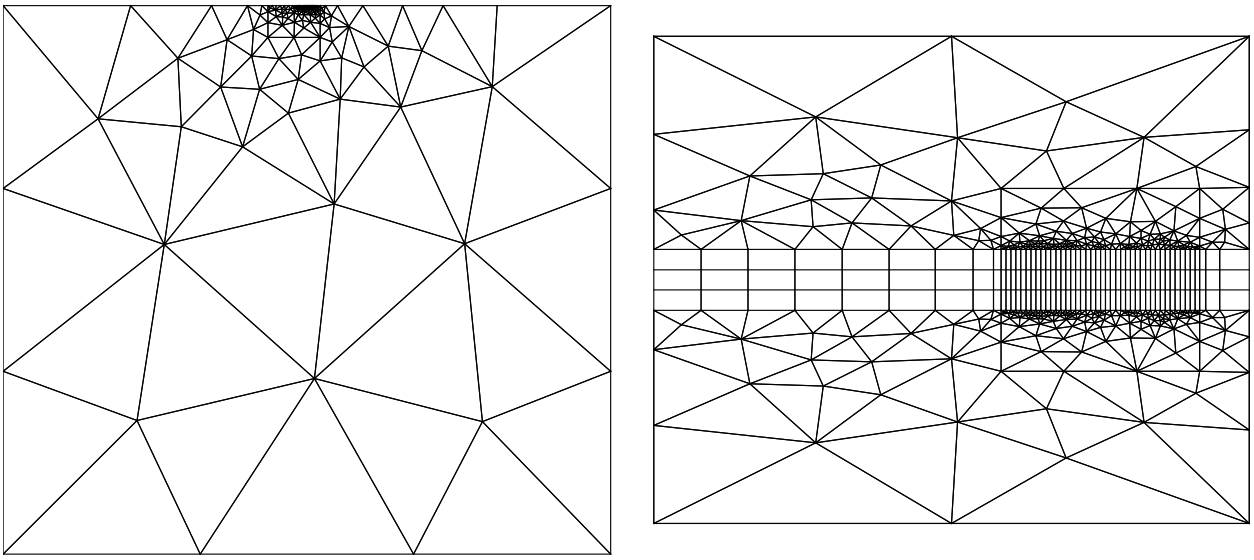

(a) EHL Domain (b) Thermal Domain

Figure 4: "*Extra Coarse*" mesh case for the EHL domain (a) and thermal domain (b)

Table 2 provides the mesh specifications for all five considered mesh cases in terms of number of elements in the 1D contact domain $\partial\Omega_c$ (n_c), number of elements in the 2D elastic domain Ω (n_e), number of elements for the 2D plane domain Ω_p in the thermal part (n_p) which is the same as the number of elements for the cylinder domain (given the mesh symmetry discussed above), the number of elements in the film thickness direction for the fluid domain of the thermal part (n_{ft}). The numbers of degrees of freedom (unknown field variables) for the hydrodynamic problem (N^h_{dof}) (which is equal to that of the shear stress problem (N^s_{dof})), the elastic problem (N^e_{dof}) and the thermal problem (N^t_{dof}) are also indicated along with the total number of degrees of freedom ($N^{tot}_{dof} = N^h_{dof} + N^e_{dof} + 1 + N^t_{dof} + N^s_{dof}$) for each mesh case.

Mesh Case	Elements				Degrees of Freedom			
	n_c	n_e	n_p	n_{ft}	N^h_{dof}	N^e_{dof}	N^t_{dof}	N^{tot}_{dof}
Extra Coarse	52	421	323	3	105	1832	1941	3984
Coarse	101	838	673	3	203	3614	3935	7956
Normal	249	2450	2116	4	499	10390	12491	23880
Fine	454	4990	4478	5	909	20982	27043	49844
Extra Fine	2114	30650	29673	10	4229	126994	203331	338784

Table 2: Mesh specifications in terms of numbers of elements and degrees of freedom

Table 2 clearly shows that the size (or number of degrees of freedom) of the hydrodynamic or shear stress problems is relatively small compared to the elastic or thermal problems. This is because the former are one-dimensional while the latter are two-dimensional.

In order to select which mesh is most adequate to attain grid-independent solutions, a mesh sensitivity analysis is carried out. For this, two typical test cases are considered: moderately and highly loaded (as detailed in table 1) with $u_m = 0.1\text{m/s}$, $SRR = 0.5$, $\mu_{2,R}/\mu_{1,R} = 0.5$ and $\alpha = 15\ \text{GPa}^{-1}$. Calculations are run on all five considered mesh cases and the results are reported in figure 5.

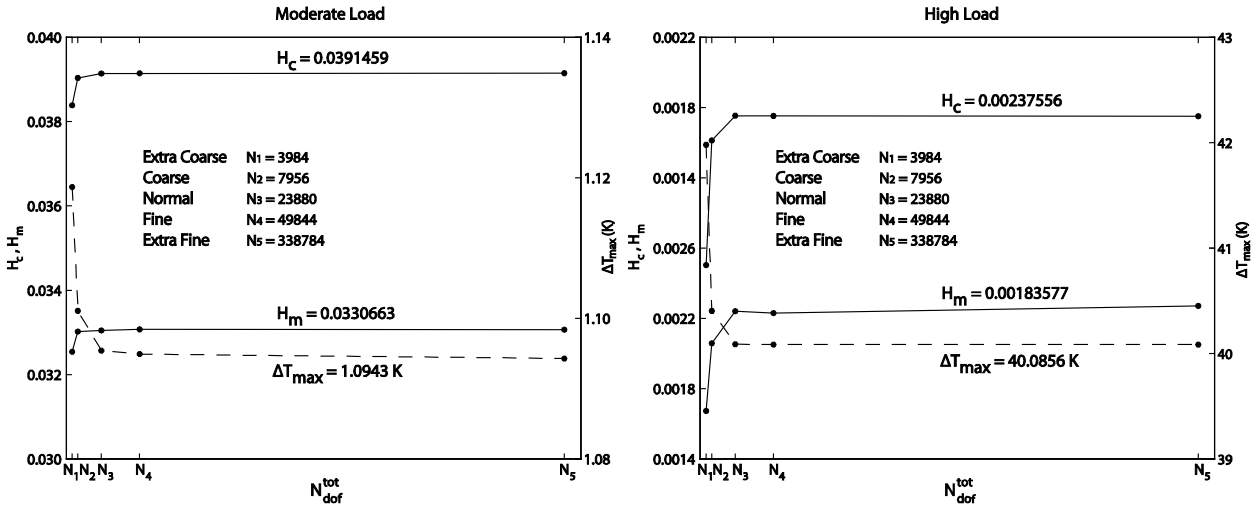

Figure 5: Film thickness and temperature convergence with respect to mesh size. Left: moderately loaded case (p_h = 0.7 GPa); Right: highly loaded case (p_h = 2.2 GPa)

Figure 5 shows the variations of dimensionless central film thickness (H_c), dimensionless minimum film thickness (H_m) and maximum temperature rise (ΔT_{max}) with mesh size for the moderately (left) and highly (right) loaded test cases. Film thicknesses are chosen to represent the convergence of the EHL part while maximum temperature rise represents that of the thermal part. It is clear form figure 5 that convergence is attained with the "*Normal*" mesh case and that any increase in the mesh density (or any further decrease in mesh size) does not lead to any meaningful improvement in the solution accuracy. So, from this point on, unless stated otherwise, the "*Normal*" mesh case is used for all calculations as it ensures grid-independent solutions with minimal memory requirements and computational overhead.

4.2. Typical Test Case Results

In this section, a typical test case with $F = 0.2\ \text{MN/m}$ ($p_h = 0.7\ \text{GPa}$), $u_m = 0.1\text{m/s}$, $SRR = 0.5$, $\mu_{2,R}/\mu_{1,R} = 0.5$ and $\alpha = 25\ \text{GPa}^{-1}$ is considered. The corresponding dimensionless pressure and film thickness distributions over the contact domain are reported in figure 6 (left). Figure 6 (middle) shows the corresponding temperature rise through the contact over the solid components' surfaces and the mid-layer of the lubricant film while figure 6 (right) shows the distribution of dimensionless lubricant shear stress over the plane's surface.

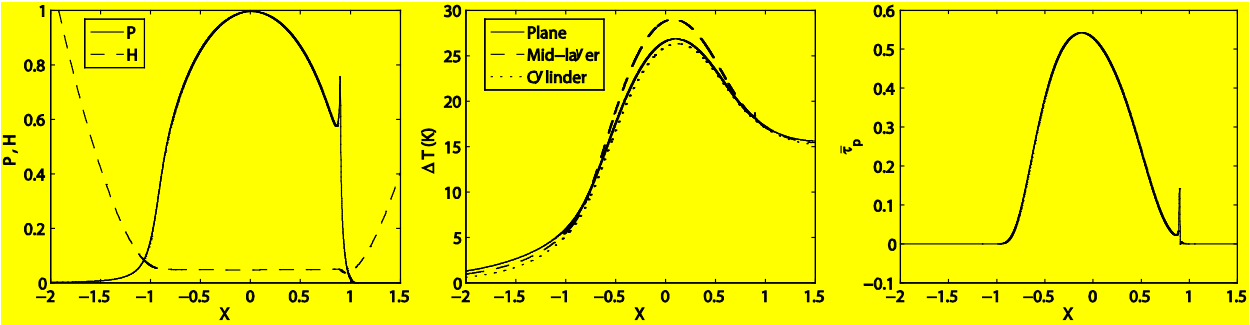

Figure 6: Dimensionless pressure and film thickness distribution (left), temperature rise over the plane's surface (Z=0), the mid-layer of the lubricant film (Z=0.5) and the cylinder's surface (Z=1) (middle) and dimensionless lubricant shear stress distribution on the plane's surface over the contact width (right) for the typical test case

The results of figure 6 show typical features of TEHL contacts such as the usual pressure spike and film thickness constriction, the temperature rise within the lubricant film which exceeds that of the solid surfaces, etc. This validates the employed approach (at least qualitatively).

4.3.Full vs Weak Coupling

Contrarily to full coupling (FC), weak coupling (WC) consists in a segregated resolution of the problem by splitting it into several parts. These are solved individually while setting the value of the field variables of the remainder parts to that obtained at the previous iteration or step. Thus, the solution of every individual part is not made intimately aware of the simultaneous evolution of the solutions of the remainder parts but rather of an "older" non-synchronized version of those. Obviously, this leads to a loss of information during the resolution process which translates into slower convergence rates. But, on the other hand, the sizes of the individual parts and their arising matrix systems become smaller requiring a reduced computational overhead for their inversion. In addition, the computation of the extra-diagonal submatrices required for a full coupling scheme is no longer required. But it remains to be identified whether or not these advantages outweigh the increased or accelerated convergence rates attained with a full coupling strategy. Four different weak coupling strategies are considered. These are detailed in the flow charts of figure 7. The iteration numbers for different loops within these strategies are denoted n_1, n_2 and n_3 as shown in figure 7. Note that the "Solve EHD Problem" block in figure 7 implies a damped-Newton resolution of the generalized Reynolds, linear elasticity and load balance equations in a fully coupled way for fixed temperature and shear stress distributions. On the other hand, the "Solve Thermal Problem" block implies a damped-Newton resolution of the energy equations for fixed pressure, film thickness and shear stress distributions while the "Solve Shear Stress Problem" implies a damped-Newton resolution of the shear stress equation (5) at every discretization point of the contact domain $\partial\Omega_c$ for fixed pressure, film thickness and temperature distributions. For all weak coupling strategies, the stopping criterion for the overall procedure is that the *L2*-norm (normalized with respect to the problem size / total number of unknowns) of the overall solution increment vector between two consecutive global iterations

falls below 10^{-6}. As for internal blocks, the stopping criteria are those of the damped-Newton procedure [41].

Note that pressure, temperature, film thickness and shear stress results are in perfect agreement among all considered coupling strategies. Given that weak coupling finite element modeling of the TEHL problem has been validated against experiments by the author and his coworkers on several occasions (e.g. [20], [42], [43] and [44]), this validates the current proposed methodologies.

The performance of the full coupling strategy is compared to that of all considered weak coupling strategies in terms of numbers of iterations required for convergence and computational (CPU) times. The pressure-viscosity coefficient for these test cases is taken to be $\alpha = 15$ GPa^{-1} while F, u_m, SRR and $\mu_{2,R}/\mu_{1,R}$ are varied. The results are reported in tables 3 and 4 respectively. Table 3 provides the numbers of iterations in outer loops and the summations of the numbers of iterations in internal loops over all outer loops for all coupling strategies while table 4 provides the corresponding overall CPU times.

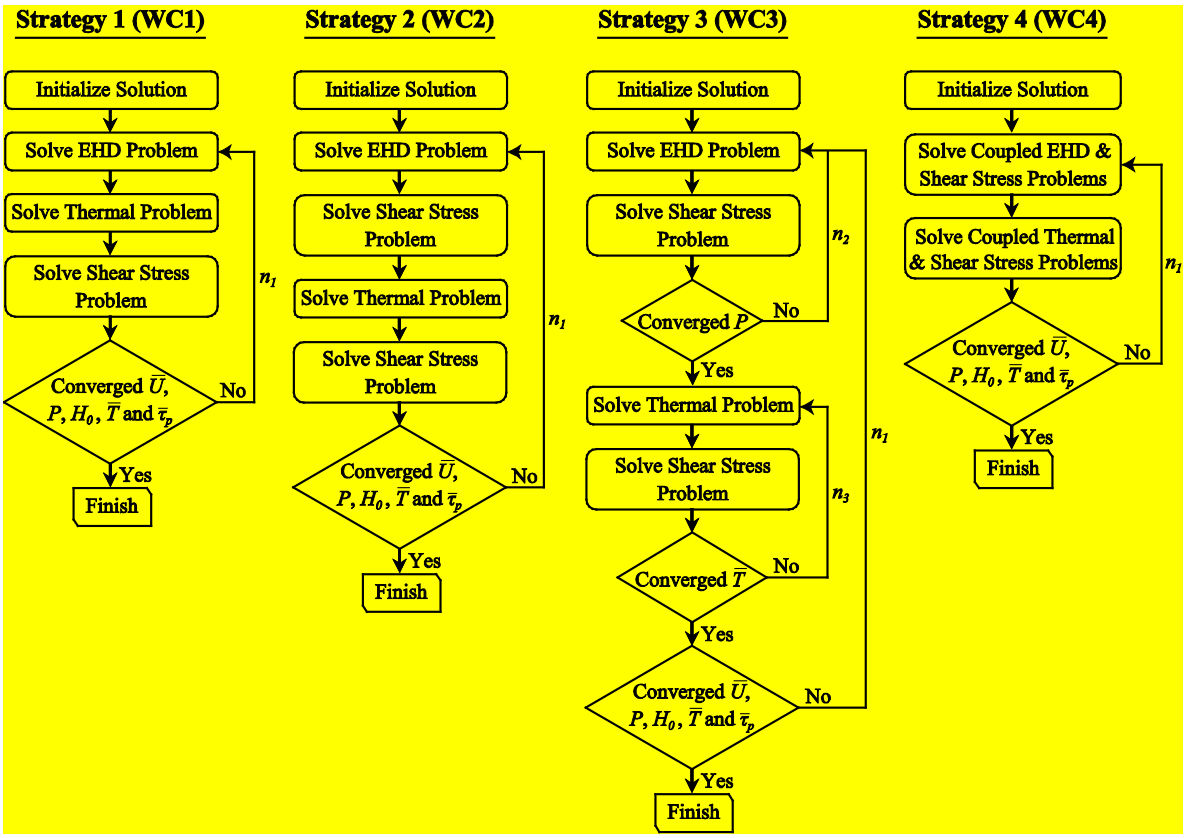

Figure 7: Flow charts of weak coupling strategies

$\frac{\mu_{2,R}}{\mu_{1,R}}$	F (MN/m)	u_m (m/s)	SRR	FC	WC1			WC2			WC3					WC4		
				n_{tehl}	$\sum n_{ehl}$	$\sum n_t$	n_1	$\sum n_{ehl}$	$\sum n_t$	n_1	$\sum n_{ehl}$	$\sum n_t$	n_1	$\sum n_2$	$\sum n_3$	$\sum n_{ehl}$	$\sum n_t$	n_1
0.5	0.2	0.1	0.0	10	14	3	3	14	3	3	21	2	2	9	2	13	2	2
			0.5	9	11	4	3	11	4	3	19	5	3	9	4	12	4	3
			1.0	8	12	4	3	12	4	3	25	5	3	13	4	15	6	4
		1.0	0.0	25	69	5	4	69	5	4	77	5	3	9	4	34	4	3
			0.5	20	29	8	4	29	8	4	65	12	4	31	7	29	8	4
			1.0	34	33	16	5	32	16	5	76	22	5	42	9	31	16	5
	2.0	0.1	0.0	25	45	4	4	45	4	4	766	2	2	200*	2	27	2	2
			0.5	28	155	12	4	124	12	4	2536	16	4	204*	7	115	15	4
			1.0	19	158	15	5	147	16	5	537	22	5	110	9	101	22	5
		1.0	0.0	27	23	5	4	23	5	4	246	5	3	206*	4	26	4	3
			0.5	26	39	39	4	27	39	4	263*	47	4	130*	9	32	39	4
			1.0	33	37	45	4	33	50	5	83	65	5	43	11	41	51	4
0.01	0.2	0.1	0.0	14	29	5	5	29	5	5	338	4	4	257*	4	16	2	2
			0.5	12	25	6	5	23	5	4	734	8	6	600*	7	16	4	3
			1.0	11	76	5	4	76	6	4	789	8	6	600*	7	15	4	3
		1.0	0.0	23	62	6	5	101	6	5	533	6	4	362*	5	102	5	4
			0.5	25	133*	9	5	39	7	4	632	11	6	464*	8	117*	7	4
			1.0	44	46	15	6	45	12	5	643	17	5	500*	9	68	10	4
	2.0	0.1	0.0	37	102	6	6	102	6	6	983	2	2	200*	2	51	2	2
			0.5	25	81	14	5	79	12	5	1522	17	4	400*	8	60	22	4
			1.0	17	68	16	6	70	15	5	1124	22	4	400*	10	52	24	4
		1.0	0.0	17	46	7	6	44	6	5	484	5	3	300*	4	30	4	3
			0.5	24	100	43	5	73	166*	6	779*	375*	5	500*	11	46	105*	4
			1.0	25	36	46	5	34	48	6	786	71	6	600*	14	29	35	4

*Internal loop convergence not attained. Iterative process of corresponding internal loop stopped when maximum number of iterations is attained.

Table 3: Comparison of numbers of iterations required for convergence of full and weak coupling strategies

$\frac{\mu_{2,R}}{\mu_{1,R}}$	F (MN/m)	u_m (m/s)	SRR	CPU (s)				
				FC	WC1	WC2	WC3	WC4
0.5	0.2	0.1	0.0	18.0	6.9	7.0	8.3	6.8
			0.5	16.0	6.9	6.9	10.2	8.3
			1.0	14.6	7.1	7.1	12.1	11.3
		1.0	0.0	43.6	46.0	46.0	48.6	17.6
			0.5	35.3	15.2	15.2	29.7	17.9
			1.0	62.1	22.8	22.6	41.4	26.4
	2.0	0.1	0.0	44.7	18.1	18.3	249.2	12.0
			0.5	50.8	72.5	58.8	1018.3	63.6
			1.0	33.9	73.8	70.3	195.9	61.7
		1.0	0.0	46.2	11.2	11.2	76.9	13.2
			0.5	67.0	84.5	79.5	176.1	84.6
			1.0	84.1	95.2	105.4	149.1	119.4
0.01	0.2	0.1	0.0	24.5	12.5	12.6	109.4	7.7
			0.5	21.1	12.2	11.0	244.6	9.7
			1.0	19.5	49.8	49.5	284.1	9.3
		1.0	0.0	39.8	31.9	73.0	193.4	39.2
			0.5	44.0	102.0	18.6	226.2	46.8
			1.0	80.8	27.7	24.8	218.8	33.6
	2.0	0.1	0.0	67.1	39.6	38.9	324.5	24.4
			0.5	46.0	37.8	35.9	546.0	43.2
			1.0	30.3	34.6	34.6	393.7	42.3
		1.0	0.0	29.3	19.9	18.6	159.7	15.0
			0.5	41.6	118.3	536.5	747.6	141.9
			1.0	61.8	76.5	86.3	389.4	68.5

Table 4: Comparison of CPU times of full and weak coupling strategies

First, comparing the different weak coupling strategies, the results of tables 3 and 4 suggest that WC1, WC2 and WC4 are more robust and efficient than WC3. These generally require an overall smaller number of iterations to attain convergence resulting in faster CPU times. In fact,

for WC3, some internal loops (which numbers of iterations are marked with a star in table 3) did not reach convergence and had to be broken when a preset maximum allowable number of iterations was exceeded. The final result though, is a converged one. This is a clear indication that stagnation points are reached within these loops, whereby the solution oscillates back and forth around a given stagnation point. This is a typical indicator of the lack of robustness of a given algorithm. This lack of robustness also appears for the other weak coupling strategies. In fact, in some cases an increased overall number of iterations and CPU times are observed for no apparent reason e.g. rows 2, 8 and 10 from the bottom in tables 3 and 4. Though sometimes no internal loops are broken as a result of stagnation, this suggests that stagnation points or slow convergence rates may be encountered within some internal loops, but these end up converging. Stagnation points are characteristic of weak coupling strategies. These are a direct result of the loss of information associated with the omission of coupling terms which are not necessarily negligible in these cases. This feature vanishes with full coupling as indicated by the results of tables 3 and 4 which reveal more consistent convergence rates and CPU times for FC strategy.

It is clear from table 3 that a full coupling strategy guarantees a smaller (and in most cases much smaller) overall number of iterations, compared to weak coupling strategies to attain convergence under all considered operating conditions. However, this doesn't always reflect into smaller CPU times. In fact, table 4 reveals that for the moderately loaded case, CPU times are generally smaller for weak coupling strategies even though the number of iterations is higher. The same applies for pure-rolling cases under any loading or mean entrainment speed conditions. This is because in both cases, the difference in the overall number of iterations between full and weak coupling strategies is not sufficiently large to compensate for the increased computational overheads associated with full coupling. These result from the introduction of additional coupling terms to be evaluated and more importantly, the inversion of a larger arising matrix system (22) compared to weak coupling strategies. This observation is not surprising as for these cases, shear-thinning as well as heat generation are relatively mild, leading to a weak dependence of the TEHL problem's solution on the thermal and shear-thinning parts. As such, the additional coupling terms are relatively negligible and have very little effect on the overall solution. Therefore, the additional computational overhead associated with their evaluation and the inversion of a larger matrix system is not justified. On the other hand, under high loading and rolling-sliding conditions, the overall number of iterations, as well as computational times become relatively smaller for the full coupling strategy compared to weak coupling strategies. This is because under such conditions, shear-thinning, as well as heat generation become significant and have a more pronounced effect on the overall solution. Thus, it becomes essential to incorporate these effects in a fully coupled way. The associated additional computational overhead in this case, is offset by the significant reduction in the overall number of iterations required for convergence.

5. Conclusion

This paper presents a finite element fully coupled approach to the resolution of TEHL problems. The approach consists in solving the governing equations: generalized Reynolds, linear elasticity, load balance, energy and shear stress equations in a monolithic system using a damped-Newton resolution procedure. The generalized Reynolds, linear elasticity and energy equations being of a partial differential nature are discretized using a finite element procedure while the load balance and shear stress equations being simple integral equations are directly added to the arising algebraic system of equations. Special stabilized finite element formulations are employed for the solution of the generalized Reynolds equation under highly loaded regime and for the solution of the energy equations under convection-dominated regime. Results clearly reveal the fast convergence characteristics associated with full coupling. In fact, solutions are attained within a few iterations only with a total computational time of one minute or less.

The performance of the proposed fully coupled scheme was compared to different weak coupling strategies. It turned out that, in some cases, weak coupling leads to a loss of robustness, resulting in a significant increase in the overall number of iterations for no apparent reason and increased CPU times. Full coupling on the other hand turned out to be very robust, with consistent convergence rates and CPU times. It guarantees a smaller (and in most cases much smaller) overall number of iterations to attain convergence, regardless of operating conditions. However, this doesn't always reflect into smaller CPU times. In fact, for moderately loaded cases, or also for pure-rolling cases under any loading or mean entrainment speed conditions, CPU times are smaller for weak coupling strategies. This is because the difference in the overall number of iterations between full and weak coupling strategies is not sufficiently large to compensate for the increased computational overheads of a full coupling strategy. Actually, for these cases, shear-thinning as well as heat generation are relatively mild, leading to a weak dependence of the TEHL problem's solution on the thermal and shear-thinning parts. As such, the additional coupling terms are relatively negligible and have very little effect on the overall solution. This being said, the additional computational overhead associated with their evaluation and the inversion of a larger matrix system is not justified. On the other hand, under high loading and rolling-sliding conditions, the overall number of iterations as well as CPU times, become relatively smaller for the full coupling strategy. This is because under these conditions, shear-thinning as well as heat generation become significant and have a more pronounced effect on the overall solution.

Nomenclature

η	: Lubricant's Generalized Newtonian viscosity (Pa.s)
$\bar{\eta}$	: Dimensionless lubricant's Generalized Newtonian viscosity
γ	: Lubricant's density-temperature coefficient (K^{-1})
$\mu_{1,R}$	: Lubricant's first Newtonian viscosity at reference state (Pa.s)

$\mu_{2,R}$: Lubricant's second Newtonian viscosity at reference state (Pa.s)

$\overline{\mu}_1$: Dimensionless lubricant's first Newtonian viscosity

$\overline{\mu}_2$: Dimensionless lubricant's second Newtonian viscosity

υ : Equivalent Poisson coefficient

υ_c : Cylinder's Poisson coefficient

υ_p : Plane's Poisson coefficient

ρ : Lubricant's density (kg/m^3)

$\overline{\rho}$: Dimensionless lubricant's density

ρ_c : Cylinder's density (kg/m^3)

ρ_p : Plane's density (kg/m^3)

ρ_R : Lubricant's density at reference state (kg/m^3)

τ : Lubricant shear stress (Pa)

$\overline{\tau}$: Lubricant's dimensionless shear stress

$\overline{\tau}_p$: Lubricant's dimensionless shear stress on plane's surface

a : Hertzian contact radius (m)

c : Lubricant's heat capacity (J/kg.K)

c_c : Cylinder's heat capacity (J/kg.K)

c_p : Plane's heat capacity (J/kg.K)

E : Equivalent Young's modulus (Pa)

E_c : Cylinder's Young's modulus of elasticity (Pa)

E_p : Plane's Young's modulus of elasticity (Pa)

F : Contact external applied load per unit length (N/m)

h : Lubricant film thickness (m)

H : Dimensionless lubricant film thickness

H_0 : Film thickness constant parameter

k : Lubricant's thermal conductivity (W/m.K)

k_c : Cylinder's thermal conductivity (W/m.K)

k_p : Plane's thermal conductivity (W/m.K)

N_P, $N_{\overline{U}}$, $N_{\overline{T}}$: Finite element weight functions for field variables P, $\overline{U}$ and $\overline{T}$

p : Pressure (Pa)

P : Dimensionless pressure

p_h : Hertzian contact pressure (Pa)

P_R : Dimensionless pressure at reference state

R : Ball's radius (m)

SRR : Slide-to-Roll ratio = $(u_c\text{-}u_p)/u_m$

T : Temperature (K)

$\overline{T}$: Dimensionless temperature

T_0 : Ambient temperature (K)

T_R : Reference temperature (K)

$\overline{T}_R$: Dimensionless temperature at reference state

$u,\ w$: x and z-components of the solid's elastic deformation field (m)

$U,\ W$: Dimensionless x and z-components of the solid's elastic deformation field

u_m : Mean entrainment speed = $(u_c+u_p)/2$ (m/s)

u_c : Cylinder's surface velocity (m/s)

u_p : Plane's surface velocity (m/s)

u_f : Lubricant's velocity field x component (m/s)

$x,\ y,\ z$: Space coordinates (m)

$X,\ Y,\ Z$: Dimensionless space coordinates

Subscripts

c: Cylinder
p: Plane
f: Fluid / Lubricant
e: Elastic
h: Hydrodynamic
l: Load balance
t: Thermal
s: Shear stress

Dimensionless Parameters

$$X=\frac{x}{a},\quad H=\frac{h\,R}{a^2},\quad U=\frac{u\,R}{a^2},\quad V=\frac{v\,R}{a^2}\quad ,P=\frac{p}{p_h},\quad \overline{T}=\frac{T}{T_0},\quad \overline{\rho}=\frac{\rho}{\rho_R},\quad \overline{\eta}=\frac{\eta}{\mu_{1,R}},\quad \overline{\tau}=\frac{\tau}{\tau_0}$$

$$Z=\begin{cases}\dfrac{z}{a}:\ \text{Solids}\\[2ex] \dfrac{z}{h}:\ \text{Lubricant Film}\end{cases}$$

References

[1] Cheng H. S. and Sternlicht B. - A Numerical Solution for the Pressure, Temperature and Film Thickness Between Two Infinitely Long, Lubricated Rolling and Sliding Cylinders, Under Heavy Loads, *ASME J. Basic. Eng.*, 1965, vol. 87, pp. 695-707.

[2] Cheng H. S. - A Refined Solution to the Thermal-Elastohydrodynamic Lubrication of Rolling and Sliding Cylinders, *ASLE Trans.*, 1965, vol. 8, pp. 397-410.

[3] Zhu D. and Wen S. - A Full Numerical Solution for the Thermo-Elastohydrodynamic problem in Elliptical Contacts, *ASME J. of Tribol.*, 1984, vol. 106, pp. 246-254.

[4] Kim K. H. and Sadeghi F. - Three-Dimensional Temperature Distribution in EHD Lubrication: Part I – Circular Contact, *ASME J. of Tribol.*, 1992, vol. 114, pp. 32-41.

[5] Guo F., Yang P. and Qu S. - On the Theory of Thermal Elastohydrodynamic Lubrication at High Slide-Roll Ratios – Circular Glass-Steel Contact Solution at Opposite Sliding. *ASME J. of Tribol.*, 2001, vol. 123, pp. 816-821.

[6] Liu X., Jiang M., Yang P. and Kaneta M. - Non-Newtonian Thermal Analyses of Point EHL Contacts Using the Eyring Model. *ASME J. of Tribol.*, 2005, vol. 127, pp. 70-81.

[7] Sharif K. J., Kong S., Evans H. P. and Snidle, R. W. - Contact and elastohydrodynamic analysis of worm gears – Part 1: theoretical formulation, *Proc. IMechE. J., Part C: J. Mech. Eng. Sc.*, 2001, vol. 215, pp. 817–830.

[8] Carslaw H. S. and Jaeger J. C. - Conduction of Heat in Solids, 1959 (Oxford University Press).

[9] Blok H. - The flash temperature concept, *Wear*, 1963, vol. 6, pp. 484–494.

[10] Hartinger M., Dumont M.-L., Ioannides S., Gosman D. and Spikes H. - CFD modeling of a thermal and shear-thinning elastohydrodynamic line contact, *ASME Journal of Tribology*, 2008, vol. 130 (4), 041503.

[11] Salehizadeh H. and Saka N. – Thermal Non-Newtonian Elastohydrodynamic Lubrication of Rolling Line Contacts. *ASME J. of Tribol.*, 1991, vol. 113, pp. 481-491.

[12] Wolff R. and Kubo A. – The Application of Newton-Raphson Method to Thermal Elastohydrodynamic Lubrication of Line Contacts. *ASME J. of Tribol.*, 1994, vol. 116, pp. 733-740.

[13] Kazama T., Ehret P. and Taylor C. M. – On the Effects of the Temperature Profile Approximation in the Thermal Newtonian Solutions of Elastohydrodynamic Line Contacts. *Proc. IMechE. J. Engnrng. Tribol.*, 2001, Part J., vol. 215, pp. 109-120.

[14] Jiang X., Wong P. L. and Zhang Z. – Thermal Non-Newtonian EHL Analysis of Rib-Roller End Contact in Tapered Roller Bearings. *ASME J. of Tribol.*, 1995, vol. 117, pp. 646-654.

[15] Lee R. T., Hsu C. H. and Kuo W. F. – Multilevel Solution for Thermal Elastohydrodynamic Lubrication of Rolling-Sliding Circular Contacts. *Tribology International*, 1995, vol. 28, pp. 541-552.

[16] Kim H. J., Ehret P., Dowson D. and Taylor C. M. - Thermal Elastohydrodynamic Analysis of Circular Contacts, Part 1: Newtonian Model, *Proc. IMechE. J. Engnrng. Tribol.*, 2001, Part J., vol. 215, pp. 339-352.

[17] Kim H. J., Ehret P., Dowson D. and Taylor C. M. - Thermal Elastohydrodynamic Analysis of Circular Contacts, Part 2: Non-Newtonian Model, *Proc. IMechE. J. Engnrng. Tribol.*, 2001, Part J., vol. 215, pp. 353-362.

[18] Kaneta M., Shigeta T. and Yang P. – Film Pressure Distributions in Point Contacts Predicted by Thermal EHL Analysis. *Tribology International*, 2006, vol. 39, n° 8, pp. 812-819.

[19] Wang Y., Li H., Tong J. and Yang P. – Transient Thermoelastohydrodynamic Lubrication Analysis of an Involute Spur Gear. *Tribology International*, 2004, vol. 37, pp. 773-782.

[20] Habchi W., Eyheramendy D., Bair S., Vergne P. and Morales-Espejel G. E. – Thermal Elastohydrodynamic Lubrication of Point Contacts Using a Newtonian/Generalized Newtonian Lubricant, *Tribology Letters*, 2008, vol. 30 (1), pp. 41-52.

[21] Habchi W., Eyheramendy D., Vergne P. and Morales-Espejel G. E. – Stabilized Fully-Coupled Finite Elements for Elastohydrodynamic Lubrication Problems, *Advances in Engineering Software*, 2012, vol. 46, pp. 4-18.

[22] Björling M., Habchi W., Bair S., Larsson R. and Marklund P. – Friction Reduction in Elastohydrodynamic Contacts by Thin Layer Thermal Insulation, *Tribology Letters*, 2014, vol. 53, pp. 477-486.

[23] Habchi W. - A Numerical Model for the Solution of Thermal Elastohydrodynamic Lubrication in Coated Circular Contacts, *Tribology International*, 2014, vol. 73, pp. 57-68.

[24] Bruyere V., Fillot N., Morales-Espejel G.E. and Vergne P. - Computational fluid dynamics and full elasticity model for sliding line thermal elastohydrodynamic contacts, *Tribology International*, 2012, vol. 46 (1), pp. 3-13.

[25] Habchi W., Eyheramendy D., Vergne P. and Morales-Espejel G. E. – A Full-System Approach of the Elastohydrodynamic Line/Point Contact Problem, *ASME Journal of Tribology*, 2008, vol. 130, 021501.

[26] Oh K. P. and Rohde S. M. – Numerical Solution of the Point Contact Problem Using the Finite Element Method. *Int. J. Num. Meth. Engnrng.*, 1977, vol.11, pp. 1507-1518.

[27] Rohde S. M. and Oh K. P. – A Unified Treatment of Thick and Thin Film Elastohydrodynamic Problems by Using Higher Order Element Methods. *Proc. Roy. Soc. London*, 1975, Part A, vol. 343, pp. 315-331.

[28] Houpert L. G. and Hamrock B. J. – Fast Approach for Calculating Film Thicknesses and Pressures in Elastohydrodynamically Lubricated Contacts at High Loads. *ASME J. of Tribol.*, 1986, vol. 108, pp. 411-420.

[29] Hsiao H. S. S., Hamrock B. J. and Tripp J. H. – Finite Element System Approach to EHL of Elliptical Contacts: Part I – Isothermal Circular Non-Newtonian Formulation. *ASME J. of Tribol.*, 1998, vol. 120, pp. 695-704.

[30] Evans H. P. and Hughes T. G. – Evaluation of Deflection in Semi-Infinite Bodies by a Differential Method. *Proc. IMechE J. Mech. Engnrng. Sc.*, 2000, Part C, vol. 214, pp. 563-584.

[31] Holmes M. J. A., Evans H. P., Hughes T.G. and Snidle R. W. – Transient Elastohydrodynamic Point Contact Analysis using a New Coupled Differential Deflection Method. Part I: Theory and Validation. *Proc. IMechE J. Engnrng. Trib.*, 2003, Part J, vol. 217, pp. 289-303.

[32] Wu S. R. – A Penalty Formulation and Numerical Approximation of the Reynolds-Hertz Problem of Elastohydrodynamic Lubrication. *Int. J. Engnrng. Sci.*, 1986, vol. 24 (6), pp. 1001-1013.

[33] Yang P. and Wen S. - A Generalized Reynolds Equation for Non-Newtonian Thermal Elastohydrodynamic Lubrication. *ASME J. of Tribol.*, 1990, vol. 112, pp. 631-636.

[34] Bair S. – High Pressure Rheology for Quantitative Elastohydrodynamics, *Elsevier Science*, Amsterdam, 2007.

[35] Roelands C. J. A. - Correlational Aspects of the Viscosity-Temperature-Pressure Relationship of Lubricating Oils, *PhD Thesis*, Technische Hogeschool Delft, The Netherlands (1966).

[36] Dowson D. and Higginson G. R. – Elastohydrodynamic Lubrication. The Fundamental of Roller and Gear Lubrication, *Oxford, Pergamon* (1966).

[37] Brooks A. N. and Hughes T. J. R. - Streamline-Upwind/Petrov-Galerkin Formulations for Convective Dominated Flows with Particular Emphasis on the Incompressible Navier-Stokes Equations. *Comp. Meth. Appl. Mech. Engnrg.*, 1982, vol. 32, pp.199-259.

[38] Hughes T. J. R., Franca L. P. and Hulbert G. M. - A New Finite Element Formulation for Computational Fluid Dynamics: VII. The Galerkin-Least-Squares Method for Advective-Diffusive Equations. *Comp. Meth. Appl. Mech. Engnrg.*, 1989, vol. 73, pp. 173-189.

[39] Galeão A. C., Almeida R. C., Malta S. M. C. and Loula A. F. D. - Finite Element Analysis of Convection Dominated Reaction-Diffusion Problems. *Appl. Num. Math.*, 2004, vol. 48, pp. 205-222.

[40] Davis T. A. and Duff I. S. - An Unsymmetric-Pattern Multifrontal Method for Sparse LU Factorization, *SIAM Journal on Matrix Analysis and Applications*, vol. 18, no. 1, pp. 140-158, 1997.

[41] Deuflhard P. – Newton Methods for Nonlinear Problems, Affine Invariance and Adaptive Algorithms. *Springer*, Germany, 2004.

[42] Habchi W., Vergne P., Bair S., Andersson O., Eyheramendy D. and Morales-Espejel G. E. – Influence of Pressure and Temperature Dependence of Thermal Properties of a Lubricant on the Behavior of Circular TEHD Contacts, *Tribology International*, 2010, vol. 43, pp. 1842-1850.

[43] Björling M., Habchi W., Bair S., Larsson R. and Marklund P. - Towards the True Prediction of EHL Friction, *Tribology International*, 2013, vol. 66, pp. 19-26.

[44] Björling M., Habchi W., Bair S., Larsson R. and Marklund P. – Friction Reduction in Elastohydrodynamic Contacts by Thin Layer Thermal Insulation, *Tribology Letters*, 2014, vol. 53, pp. 477-486.